Rath *et al.*
Journal of Engineering and Applied Science (2022) 69:117
https://doi.org/10.1186/s44147-022-00169-2

Journal of Engineering and Applied Science

RESEARCH Open Access

Effect of different geometric factors of H-shaped steel section on bi-axially loaded fully encased composite column

Badrinarayan Rath[1*], Feven Kiflu[1], Bewiket Dereje[1], Shiferaw Garoma[1], Kassahun Kebede[1] and Endalkachew Mosisa Gutema[2]

*Correspondence: rath_rcpit@rediffmail.com

[1] Civil Engineering Department, Wollega University, Nekemte, Ethiopia
[2] Mechanical Engineering Department, Wollega University, Nekemte, Ethiopia

Abstract

A parametric study was conducted to investigate the influence of geometric factors on the fully encased composite column under eccentric loading about both axes of the steel section by using ABAQUS software. Thirty-six column specimens were assembled under 9 different groups by considering types of length to depth ratios (L/D ratios), three types of eccentricity to depth ratios (e/D ratios), and three types of steel contribution ratios. For validation of the model, simulations were conducted for eccentric loaded composite column test specimens from current studies and published literature. These composite columns were simulated under eccentrically applied axial load to observe the ultimate load carrying capacity, failure behavior, and axial deformation under ultimate load. Generally, these were found to greatly influence to ductility and load carrying capacity of fully encased composite column specimens. It was found that the axial load carrying capacity of the composite column was reduced with an increment of the L/D ratio up to 35%. As the e/D ratio was increased, the flexural stiffness of the column was reduced gradually. The increment of the structural steel contribution ratio increased the ductility and load-carrying capacity with a smooth decline of the post-peak region of the curve. A load-Moment interaction diagram was plotted based on EBCS EN 1994-1-1:2014 from test results.

Keywords: Geometric factors, Eccentric load, Load-moment interaction diagram, Composite column, Finite element method

Introduction

A composite column is one of the structural members, which is a combination of concrete and structural steel of any shape with or without reinforcing steel bars to provide adequate load carrying capacity to sustain both axial and eccentric loads. The structural steel may be solid, pipe, or tube. The integral and interactive behavior of structural steel and concrete makes the composite column more ductile, stiff, and cost-effective. Both the concrete and steel sections resist external loading due to effective bonding and high friction. In earlier days people are improving the strength and durability of concrete structures by using supplementary cementitious materials, organic admixtures,

changing the mix design process, wrapping the fiber-reinforced polymer, etc. But nowadays composite columns are worldwide popular for the construction of high-rise buildings since it reduces the size of the column structure and increases the usable space of the floor plan. In addition, the composite column provides significant shear resistance to strong seismic loads and other lateral loads. There are three types of composite column sections used for high-rise buildings. They are fully encased composite column (FEC), and partially encased composite column (PEC) concrete-filled tube (CFT). Among these three sections, fully encased composite column provides corrosion protection and better fireproofing because the steel section is fully covered by concrete. The load-carrying capacity of the composite column depends upon length to depth ratio (L/D ratio), eccentricity to depth ratio (e/D ratio), and structural steel contribution ratio (δ). The slenderness of the column depends upon the L/D ratio. Recently, the structural behavior of slender steel composite columns became a major concern for design engineers. In earlier days Mirza and Skrabek (1991) [1]. Wu et al. (2019) [2], and Lu et al. (2015) [3] studied short concrete steel composite column under axial load whereas Tokgoz et al. (2012) [4], Shanmugam and Lakshmi (2001) [5] reported about the slender composite column under eccentric loading. In recent years, several studies on composite columns have been demonstrated by using different software. An H-shaped steel column section confined with concrete was analyzed by ABAQUS under a combination of axial load and the bending moment [6]. Different confinement regions were introduced such that the numerical model would give a good agreement with experimental results. It was concluded that predictions of the American Institute for Steel Construction were quite conserved. Besides to H-shape steel section, other shapes such as I-shape, T-shape, and Cross shape were analyzed by numerical method for observation of composite section behavior for the steel sections and longitudinal reinforcement [7]. It was found that axial load carrying capacity and forced deformation behavior for both experimental and numerical methods coincided with each other. Also, the structural steel sections and lateral reinforcement enhanced the post-peak strength. Both EN 1994-1-1:2004 [8] and JGJ 138-2016 [9] codes were modified inscribing slenderness parameters and various load factors with the help of regression analysis [10]. Various dynamic characteristics such as natural frequencies, mode shapes, and damping ratios of the fully encased composite column under cyclic loading test was investigated by both experimental and numerical methods [11]. The results found that the damage at the connection zones of the column and beam were the main cause for the distinctly decreasing natural frequencies. A numerical study had carried out about the drop weight (geometric shape of impactors) and its effects on the weak axis of rectangular hollow steel beam sections under the impact loading [12]. It was noticed that the maximum acceleration and deflection had occurred in beams, stroked by the triangular-headed impactors. By using of the triangular headed impactor, a high amount of stress distribution and plastic deformation had been observed. The impactor was modeled with C3D8R finite element by ABAQUS. A finite element analysis model was developed for the prediction of concrete encased CFST box stub columns under axial loading [13]. Various parametric studies had been investigated for the influence of strength of steel and concrete, longitudinal bar ratio, the ratio between sectional width and diameter of CFST, spacing of stirrups, steel ratio of CFST, etc. Partially encased composite columns were investigated by numerical methods

subjected to eccentric loading [14]. It was concluded that the existing design methods prescribed by Eurocode 4 could be unconservative under certain circumstances. Also, it was noticed that increasing the width of the flange to the thickness of the flange ratio and the width of the flange to the thickness of the web ratio, increased the axial load carrying capacity of the composite column [15]. By investigating of behavior of square tubed steel reinforced concrete under eccentric compression, it was noticed that the initial buckling of the tube occurred for the ultimate value of load when the B/t ratio is 100. But the buckling occurred earlier when the B/t ratio was 133 when the load reached 88 to 94% of the ultimate load [16]. Experimental research was carried out on composite columns subjected to fire under several parameters such as rotational and axial restraining to thermal elongation, different levels of applied load, and different slenderness values of the column [17]. The collected data of EN 1994-1-2 (2005) showed very conservative as compared to the experimental test. The fully encased steel-concrete composite column had higher energy absorption capacity when the columns were cast with high-strength concrete. These types of columns had been recommended for the construction of the seismic area, even if the failure mode was brittle [18]. When the axial compressive load was applied to a plastic pour-in form type composite column a hinge was formed and the brittle shear failure changed to ductile failure [19]. The necessity for more numerical and experimental studies on the behavior of composite columns subjected to axial loading for different parameters.

Research significance

Buckling under eccentric loading is the main disadvantage of a steel column. It has been found that when the concrete is filled on the outer periphery of the H-shape steel column, the web components are better restrained than the flange component due to the less occupied area of the web portion. If the flange has not acquired a sufficient width-to-thickness ratio, then there are chances to undergo local buckling. The buckling of the column depends upon several factors such as L/D ratio, e/D ratio, encased steel contribution ratio, amount of longitudinal reinforcement and transversal reinforcement, spacing of ties, the strength of concrete and steel. Among them, some factors have been discussed by many researchers, and some factors are remained to discuss. In this research, three types of rolled steel H-section have been encased inside the four types of a cross-section of composite column applied under different eccentric loadings. The buckling of column, load carrying capacity, and failure envelope of the composite column were studied under several factors such as L/D ratio, e/D ratio, and steel contribution ratio by ABAQUS software. The novelty of the present research is an analyzation of the ultimate load moment interaction diagram for composite columns centrally encased with three different yield strength rolled steel H-Section in a higher depth. According to the position of the neutral axis the ultimate bending moment has been calculated for a composite beam centrally encased with an H-section. Also, limited research has been carried out for ultimate load-carrying capacity and bending moment analysis under the factors of L/D ratio, e/D ratio, and steel contribution ratio. The aim of the study is to investigate the influence of geometric factors (such that L/D, e/D, and steel to concrete ratio) on the fully encased composite column under eccentric loading about major and minor axes. Modeling and validating work were conducted through ABAQUS software

so that it can be easier to use the proposed model for further investigation. The objectives of the present study are

(i) To conduct a numerical investigation on a fully encased composite column under several eccentric loadings with different eccentricities.
(ii) To perform the parametric study to explore the effect of several factors such as L/D ratio, e/D ratio, and steel contribution ratio.
(iii) To study the effect of L/D ratios on the second-order moment of the composite column.
(iv) To draw the load-moment interaction diagram from the results of ABAQUS analysis.

Methods

The influence of various parameters such as L/D ratio, structural steel contribution ratio (δ), eccentricity to depth ratio (e/D), and spacing of transverse reinforcement (S), on fully encased composite columns with various L/D ratios had been investigated. In the present research, the structural steel contribution ratio means the area of rolled steel section (H-shaped steel section) to the total area of the composite column. The longitudinal bars of 16 mm diameter were inserted at four corners of the composite column and the transversal link of 8 mm diameter was used. The total area of longitudinal bars was very small as compared to the area of rolled steel section. Hence the total area of the longitudinal bar had been decided not to consider in the structural steel contribution ratio. A total of 36 specimens of fully encased composite columns samples were assembled with different L/D ratios and the load carrying capacity of the above specimen had been analyzed with the help of finite element software ABAQUS. The typical view of the composite column section in the present research is shown in Fig. 1. The composite columns include components such as concrete columns, longitudinal reinforcement, and transversal links that were modeled using a combination of solid elements, truss elements, and shell elements. The modeling process of different parts of the composite column by ABAQUS software has been shown in Fig. 2. The S4R shell element was used for modeling of the structural steel section, which has six degrees of freedom. They are three translations and three rotations. There are five elements for the default number of integration points, which were sufficient for modeling the non-linear material behavior of the composite columns. The concrete column was simulated using a solid C3D8R element. Both top and bottom parts of the column were placed with two rigid plates to simulate the real condition of the composite column. They were modeled using a 3D four-node bilinear discrete rigid shell element. The various parts (concrete beam, longitudinal bar, tie bars, etc.) of the composite column were meshed individually and assembled for further process. The mesh size of 50 mm was selected for all components of the present composite column. The composite column specimen under the present study had a pin-ended end condition. This type of end condition was achieved by allowing rotational degrees of freedom around the major axis for both reference points at direction x-x, and axial displacement at the loaded end direction z-z. The different stages of ABAQUS modeling are shown in Fig. 3. The length of all columns was taken as 3 meters and four types of L/D ratios (10, 12, 15, and 20) had been introduced by taking

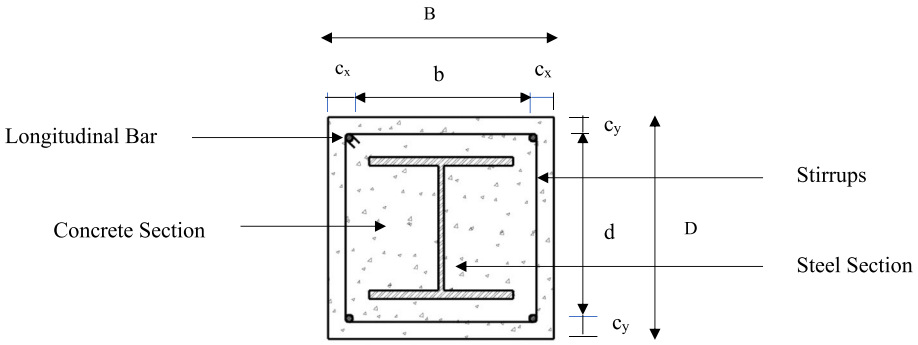

(a) Sectional View of Composite Column Section

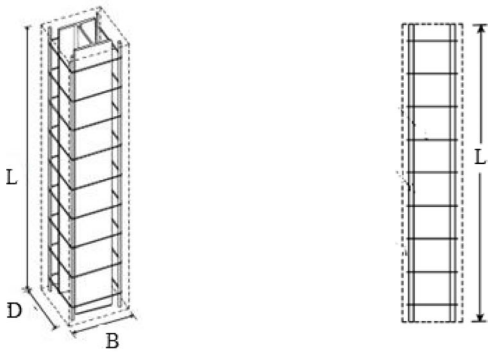

(b) Elevation of Composite Column Section

Fig. 1 Geometry of composite column specimen

four types of the cross-section. The analysis was carried out on the three types of rolled steel H-section (HEB 200, HEB 220, and HEB 240) to see the structural steel contribution ratio (δ). The grade of concrete was considered as C35/45. A static load had been applied to the column by taking three types of eccentricity ratios in both directions (i.e., 0.1, 0.3, 0.5). The detailed specifications of 36 columns are shown in Table 1. The overall soundness of the long column depends upon the L/D ratio of the column. The diameter of main and transverse reinforcement was 12 mm and 8 mm respectively. The L/D ratio of 12 has been marked as a boundary line between short and long columns by many researchers [20–22]. To simulate the various structural member through ABAQUS several material properties such as mechanical, thermal, electrical, and mass diffusion have to be fed as input parameters. Among them, the concrete damage plasticity model and the concrete smeared cracking model are very essential to simulate the concrete material behavior like an elastic response, plastic response, damage, and failure in the long fully encased composite column.

The concrete damaged plasticity (CDP) model used in ABAQUS software is a plasticity-based model which arranges to analyze concrete structures under arbitrary loading conditions [23]. For the present research, the CDP model was prepared from a laboratory test. The material mechanical properties used in the finite element model are described in Table 2. The stress-strain behavior of concrete and steel is shown in Fig. 4.

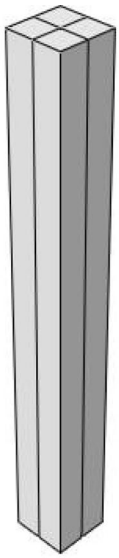

(a) Concrete Column Section

(b) Longitudinal Reinforcement

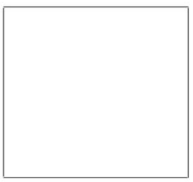

(c) Transversal Reinforcement

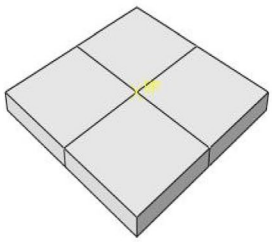

(d) Supporting Steel Plate

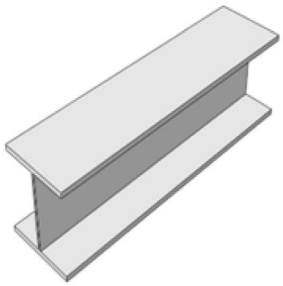

(e) Structural Steel Section

Fig. 2 ABAQUS modeling for different parts of composite column

In the present study, the elastic-plastic model was used to define the properties of steel such as H-shaped rolled steel section, longitudinal reinforcement, and transverse reinforcement as per EBCS EN 1994-1-1,3.3:2014 [24]. The mechanical properties of the structural steel section and the reinforcement bars utilized in the present study are shown in Table 3.

The structural steel section, longitudinal and transverse reinforcement, and concrete columns were molded with S4R shell element, truss element, and solid element respectively. To simulate the real conditions of the long columns, two numbers of rigid plates were kept at the top and bottom face of each column. They were molded by using 3D four-node bilinear discrete rigid shell elements (R3D4). The mesh size of 50 mm was selected for the different components of long columns in order to produce the

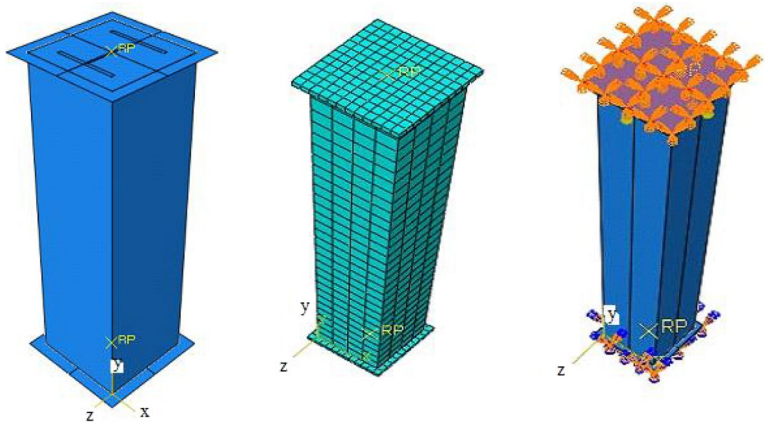

(a) Modelling of Composite Column (b) Meshing of Composite Column (c) Application of Boundary Condition

Fig. 3 Different stages of modeling by ABAQUS software

accurate behavior of a fully encased composite column with less computational time. The embedded element constraint technique was used to specify the group of elements embedded in the "host" element. In this research, the concrete was defined as the host element and both longitudinal and transverse reinforcement were defined as the embedded element. For the bond between concrete and structural steel, H section a "Tie" constraint pair was set, at which concrete was acting as the master surface and H-section was acting as the slave surface. Pin-ended end conditions had been applied to all column specimens, studied in this investigation. Two reference nodes were placed at the bottom and top of the rigid plates. The axial load was applied by using the displacement control technique in increments through the top rigid body. Before going to analysis, the finite element modeling of long fully encased composite columns under biaxial loading was validated by a previous experimental study [25]. The finite element analysis results were compared with the previous experimental results in terms of peak load and load-deflection response. It was observed that the present numerical model was able to predict the experimental load-deflection curve behavior with high accuracy. The failure mode from the ABAQUS and experimental analysis is illustrated in Fig. 5.

Results and discussion

In total, 36 long fully encased composite columns were assembled with normal strength concrete and normal strength steel under eccentric loading in ABAQUS and simulated to examine their strength and behavior. All specimens were loaded up to the failure. The potential input variables were L/D ratio, structural steel contribution ratio (δ), and eccentricity to depth ratio (e/D). Buckling behavior, load-moment relationship, ultimate load carrying capacity, the corresponding moment at peak load, and failure modes were the output parameters that were to be investigated.

Table 1 Specifications for different column specimen

Groups	Column ID	B × D	L/D	e_x/D	e_y/D	Steel structure
Group 1	C1	250 × 250	12	0.1	0.1	HEB 200
	C2	200 × 200	15	0.1	0.1	
	C3	150 × 150	20	0.1	0.1	
	C4	120 × 120	25	0.1	0.1	
Group 2	C5	250 × 250	12	0.3	0.3	
	C6	200 × 200	15	0.3	0.3	
	C7	150 × 150	20	0.3	0.3	
	C8	120 × 120	25	0.3	0.3	
Group 3	C9	250 × 250	12	0.5	0.5	
	C10	200 × 200	15	0.5	0.5	
	C11	150 × 150	20	0.5	0.5	
	C12	120 × 120	25	0.5	0.5	
Group 4	C13	250 × 250	12	0.1	0.1	HEB 220
	C14	200 × 200	15	0.1	0.1	
	C15	150 × 150	20	0.1	0.1	
	C16	120 × 120	25	0.1	0.1	
Group 5	C17	250 × 250	12	0.3	0.3	
	C18	200 × 200	15	0.3	0.3	
	C19	150 × 150	20	0.3	0.3	
	C20	120 × 120	25	0.3	0.3	
Group 6	C21	250 × 250	12	0.5	0.5	
	C22	200 × 200	15	0.5	0.5	
	C23	150 × 150	20	0.5	0.5	
	C24	120 × 120	25	0.5	0.5	HEB 240
Group 7	C25	250 × 250	12	0.3	0.1	
	C26	200 × 200	15	0.3	0.1	
	C27	150 × 150	20	0.3	0.1	
	C28	120 × 120	25	0.3	0.1	
Group 8	C29	250 × 250	12	0.5	0.3	
	C30	200 × 200	15	0.5	0.3	
	C31	150 × 150	20	0.5	0.3	
	C32	120 × 120	25	0.5	0.3	
Group 9	C33	250 × 250	12	0.5	0.5	
	C34	200 × 200	15	0.5	0.5	
	C35	150 × 150	20	0.5	0.5	
	C36	120 × 120	25	0.5	0.5	

Table 2 Parameters used in CDP model

Parameter	Φ	ε	f_{b0}/f_{c0}	K	μ
Value	35	0.1	1.16	0.667	0.007985

Effect of L/D ratio

The buckling of column members was found when the members under compressive force became unstable due to the higher value of the L/D ratio and the high magnitude of the applied load. The mid-height deflection of various composite columns due

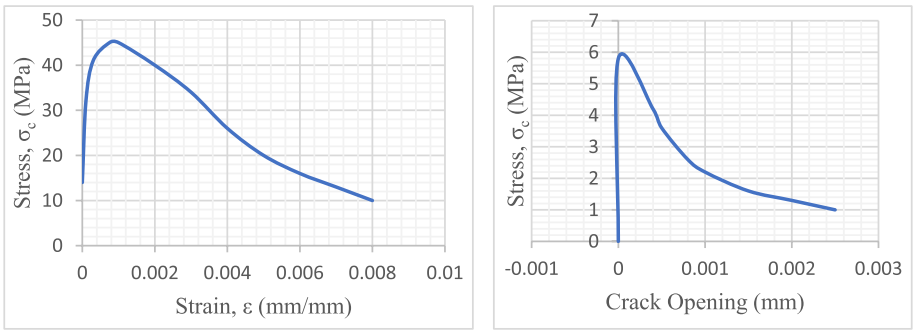

Fig. 4 Stress-strain curve for compressive and tensile behavior of concrete

Table 3 Mechanical properties of steel section and reinforcement bars

Material	Yield stress (MPa)	Ultimate stress (MPa)	Density (kg/m^3)	Young's modulus (GPa)	Poisson ratio
HEB 200	235	360	7850	210	0.3
HEB 220	275	430	7850	210	0.3
HEB 240	355	490	7850	210	0.3
Reinforcement bar (12 mm Φ and 8 mm Φ)	500	545	7850	200	0.3

to eccentric load is shown in Fig. 6. It was observed that the mid-height deflection of the composite column was increasing and load carrying capacity was decreasing with increasing in L/D ratio. It had been found that the deflection value is showing more for an e/D ratio of 0.3 than another e/D ratio of the same L/D ratio. This was due to the increase of compressive strain on one side of the column and then the other side as a result of increased curvature. The load-carrying capacity of the composite column encased with HEB 240 and lower e/D and L/D ratio was higher than the other column specimen. The load-carrying capacity of column C25 is more than 3.5 times of column C12. Local buckling of flanges was observed at the mid-height of the specimen. When the local buckling occurred at the mid-height, high stresses and strains were developed in the corner areas. The strain localization near corner areas was leading to inelastic buckling. The resisting capacity of the composite column decreased in the post-buckling phase, after attaining the maximum buckling load. When the load level reached 40% of the ultimate capacity of steel section HEB 240, i.e., 2500 kN, the first crack appeared in the middle of the front face of the column. As the load was increased, the horizontal cracks appeared at the tension side of the column when the load level reached 4500 kN. Due to excess bending moment, the mid portion of the column had deflected towards the right side. The concrete of the compressive zone started to crush after reaching the peak load of 5500 kN, and the tensile zone was filled with horizontal cracks. It was found that the load carrying capacity was gradually decreasing as the vertical deflection developed. The analysis through ABAQUS was continued till for getting a large horizontal deflection at the mid-height.

The load carrying capacity (P_{FEA}) for the first three groups of HEB 200 steel structures was found from the ABAQUS analysis (finite element analysis) as shown in Table 4 and

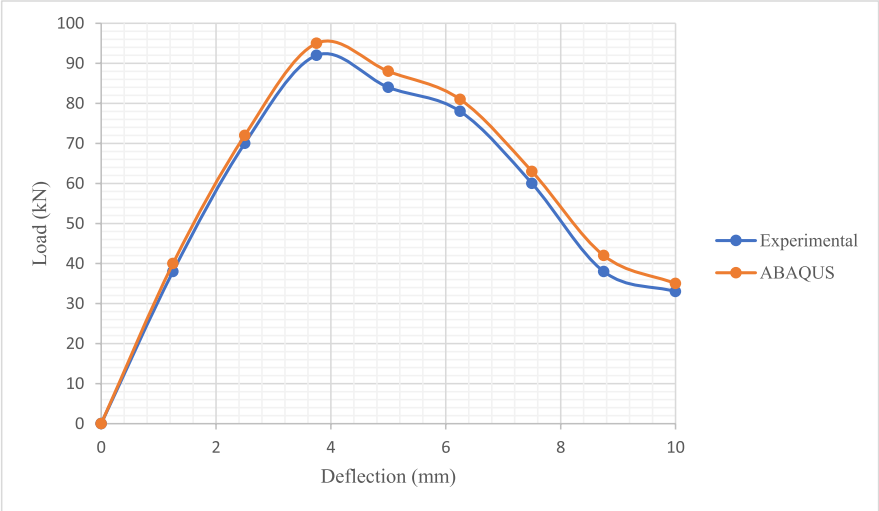

(a) Load Deflection Curve for both Experimental and ABAQUS Analysis under Axial Load

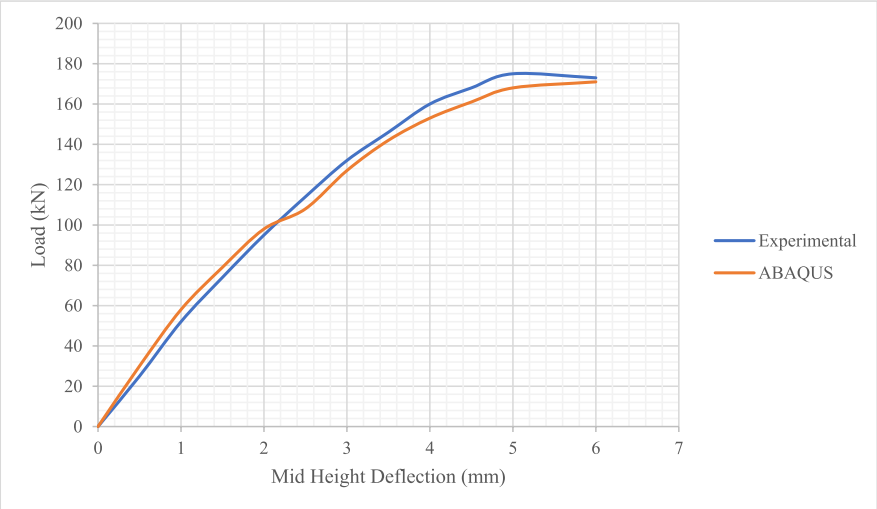

(b) Load Displacement curve for both Experimental and ABAQUS Analysis under Biaxial Bending

Fig. 5 Load displacement curve for both experimental and ABAQUS analysis

compared with the factored strength predicted by EBCS EN1994-1-1: 2014 [24]. It has been noticed that the load carrying capacity obtained from the Finite Element Analysis is less than the factored strength predicted by EBCS EN1994-1-1: 2014 except for an L/D ratio of 25. It indicates that beyond the L/D ratio of 20, ABAQUS is not showing the exact buckling of the composite column. Similar results were found for the other two types of steel structures, i.e., HEB 220 and HEB 240. Looking at the comparisons between the composite column's strength obtained from finite element analysis and the design code of EBCS EN1994-1-1: 2014, it can be concluded that the predictions of this code are quite conservative.

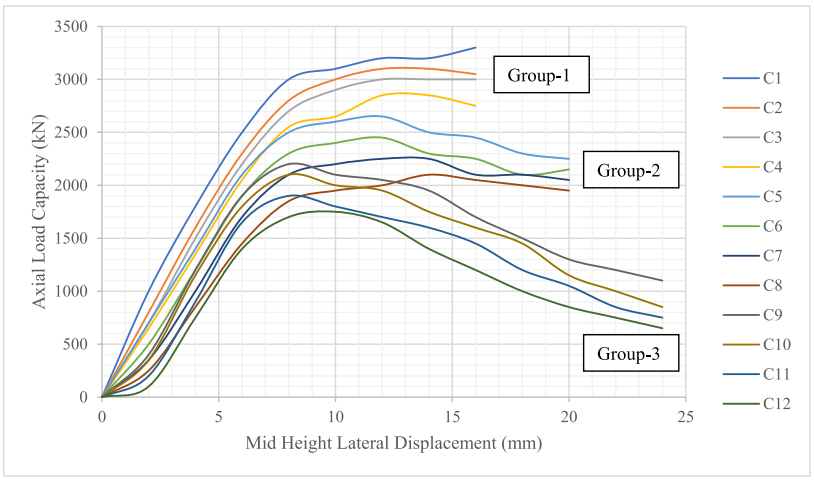

(a) Load Lateral Displacement Curve for Steel Section HEB 200

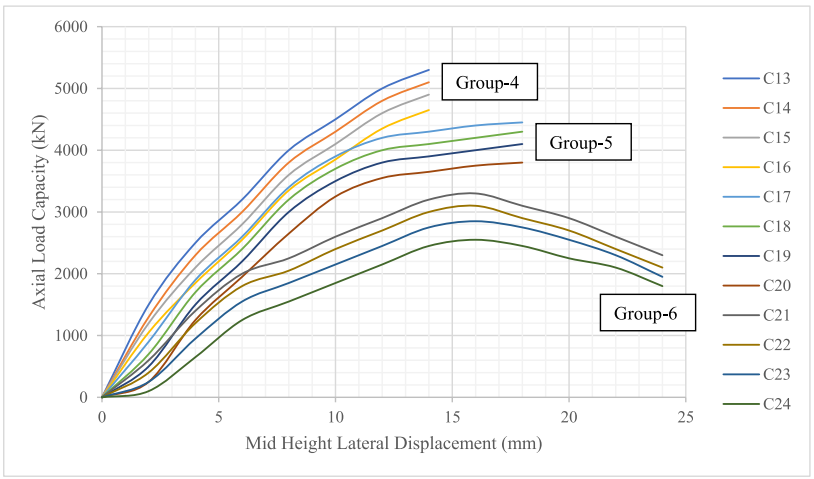

(b) Load Lateral Displacement Curve for Steel Section HEB 220

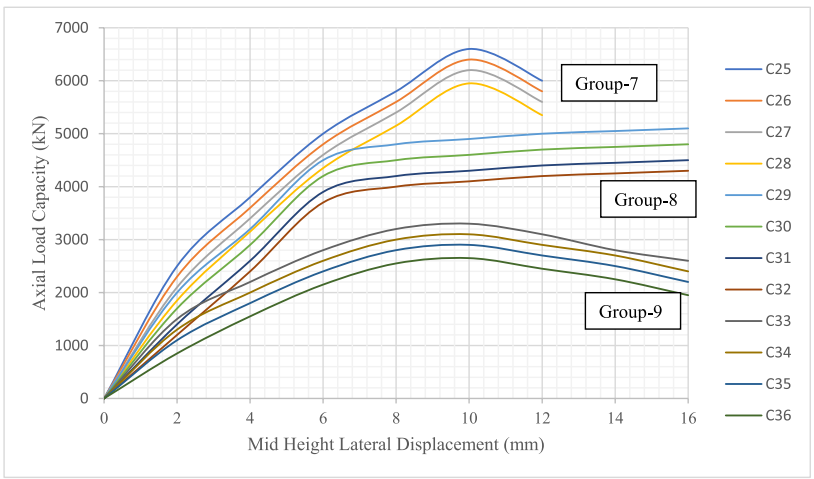

(c) Load Lateral Displacement Curve for Steel Section HEB 240

Fig. 6 Load lateral displacement curve for various steel sections

Table 4 Comparison of load carrying capacity between ABAQUS analysis and EBCS EN 1994-1-1: 2014 prediction formula

Group *No*	L/D ratio	P_{FEA}	P_{ESEN4}	P_{FEA}/P_{ESEN4}
Group 1	12	3993.81	4341.07	0.91
	15	3468.09	3557.83	0.97
	20	2630.04	2815.55	0.93
	25	2226.58	2150.9	1.03
Group 2	12	4985.45	5078.16	0.98
	15	4024.61	4152.14	0.97
	20	3279.71	3285.87	0.99
	25	2669.57	2509.2	1.1
Group 3	12	5517.79	5539.13	0.99
	15	4399.9	4444.98	0.98
	20	3185.69	3282.45	0.97
	25	2428.27	2393.45	1.01

Effect of e/D ratio

The behavior of fully encased composite slender columns under bending was highly influenced by the initial load eccentricity ratio. Due to the increase of higher e/D ratios, the flexural compression in the cross-section had increased and reduced the load carrying capacity of the column. The impact of eccentricity on the load-lateral displacement response for slender columns is shown in Fig. 6. It was found that as the e/D ratio was increased, the flexural stiffness of the column was reduced gradually. Columns with a small e/D ratio were showing the same ductile behavior with high flexural stiffness. A nonlinear load-displacement curve was observed for the columns for a higher e/D ratio of each type of steel section and it was a lower value due to the increment of mid-height second-order displacement. A linear ascending load-deflection curve was seen for the column of both e/D ratios 0.1 and 0.3. However, a relatively flat curve was found for the column sample of e/D ratio 0.3 (group 2, group 5, and group 8) whereas the flatness was absent for the columns of e/D ratio 0.1. This flatness behavior with mild slope was seen for the columns group 8). A linear ascending load-deflection curve accompanied by a sharp decline in post-peak behavior was observed for the columns of group 7. At low eccentricity, the cover spalling was mild and slow, which was leading to a less brittle failure. As the eccentricity was increasing, the cover spalling was quick and rough and leading to a brittle catastrophic failure.

Effect of structural steel contribution ratio

In the present research, three different structural steel contribution ratios said 44%, 52%, and 62% by using three different types of steel sections HEB 200, HEB 220, and HEB 240. Those structural steel contributions had been investigated to examine their effect on the strength and behavior of slenderer fully encased composite columns in the present research. It was noticed that the structural steel contribution ratio highly influenced the load-carrying capacity of the columns and their behavior. When the structural steel contribution ratio increased the ductility, as well as load carrying capacity of the column, was enhanced with a smooth decline of the post-peak region of the curve. Columns with lower structural steel contribution ratios had shown a sudden decline in the post-peak load lateral deflection curve. The bending moment reported in

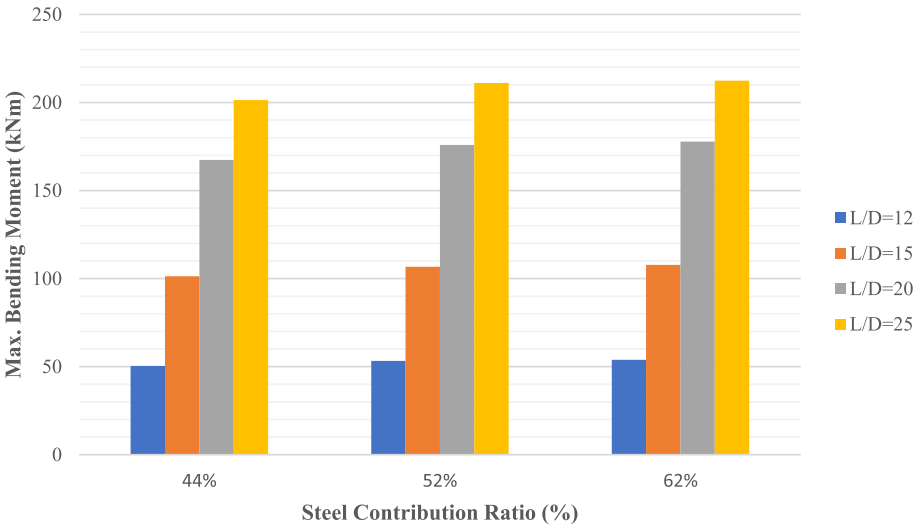

Fig. 7 Effect of structural steel contribution ratio on maximum bending moment for eccentricity of 0.3

Fig. 7 consists of the first moment calculated based on an initial eccentricity of 0.3 and the maximum bending moment caused by lateral mid-height displacement at the peak load. It can be pointed out that the axial load produced a large bending moment at the mid-height of the column and its initial eccentricity of the loading in the second-order effect. The ultimate load carrying capacity was enhanced by 0.56% and 5.14% when the structural steel contribution ratio was increased to 52% and 62% respectively, compared with that of the column with a structural steel contribution ratio of 44%. When the structural steel contribution had increased from 44 to 52% and 62% respectively, the corresponding bending moment was increased by 0.61% and 5.17% respectively. It indicates that the structural steel contribution ratio had significantly influenced the strength and behavior of the slender fully encased composite column. Similar types of observations were found for other steel contribution ratios.

Load versus moment response

Since an eccentric compressive force was acting on the column specimens, an additional bending was developed in the member. The produced internal bending moment was larger than the predicted bending moment on the undeflected structure. The analysis of a structure involving second-order effects depends upon the deformed geometry. The second-order analysis provides the deflection of a structure due to the external load and determines the effect of deflection on the internal forces generated. The second-order effect is generally employed for the verification of the stability of the steel structure. According to EBCS EN 1994-1-1: 2014, second-order effects can be neglected if the load factor for elastic instability exceeds 10. The load factor is nothing but the ratio between the elastic critical load and the corresponding applied to load. The second-order effects can be found by using the following formula [25].

$$M_{x,Ed,II} = K_1 M_{x,Ed,I} + K_2 M_{x,Ed,Imp} \quad (1)$$

Where

$$K_1 = \frac{0.66}{1 - \frac{N_{Ed}}{N_{cr,xeff}}} \text{ and } K_2 = \frac{1.0}{1 - \frac{N_{Ed}}{N_{cr,xeff}}}$$

Again

$$N_{cr,xeff} = \frac{\pi^2 (EI)_{eff}}{L^2}$$

The second-order moment was determined by using Eq. (1) and shown in Fig. 8. It was found that the second order moment of composite columns was highly increased as the L/D ratio of that column had increased. The second order moment for an L/D ratio of 12 found as very less as compared to the L/D ratio of 25. Those columns having a large value of L/D ratio exhibited a large value of mid-height lateral displacement than the columns with lower L/D ratios. The second moment of inertia for the L/D ratio of 25 for the group 3 column found as highest value compared to others. This happened due to the application of load with high eccentricity on a small cross-sectional area of the column. Due to this, the buckling resistance was decreased. It was noticed that as the grade of steel increased the second order moment value decreased. The second order moment was half for HEB 220 and one-fourth for HEB 240 with respect to HEB 200. The total moment for the column specimens with a lower L/D ratio was governed by the moment due to initial eccentricity. However, as the L/D ratio increased, the second order effect was included and the behavior changed into a nonlinear pattern because of large deflection. Since the variation of the total moment did not find as uniform, it is quite difficult to discuss the effect of the slenderness ratio on the total moment at the peak load. Because the columns with a higher L/D ratio are governed by the second order displacement.

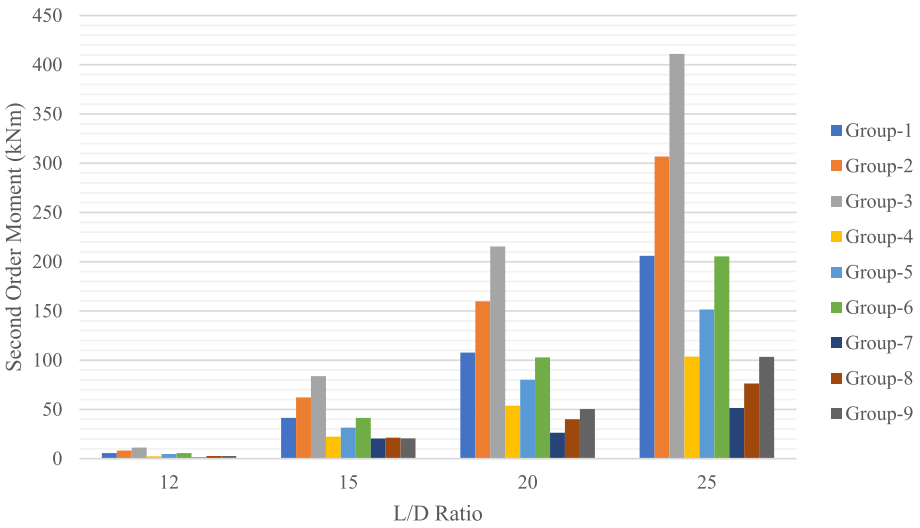

Fig. 8 Effect of slenderness ratio on the second order moment

Load versus moment curve of fully encased composite column based on EBCS EN 1994-1-1:2014

The load moment interaction curve is the locus for the cartesian coordinate of moment and load which defines the limits of strength of the cross-section of column structure under combined compression and bending. The interaction diagram has been constructed for bending the major axis and minor axis based on plastic stress distribution equations given by EBCS EN 1994-1-1:2014. The reduction factor of strength and effect of slenderness was not considered for the plotting of these curves. The load moment curves were generated for the normal strength of materials and columns of HEB 200, HEB 220, and HEB 240. From the numerical analysis, the ultimate load-carrying capacity was determined. The plastic stress distribution of a fully encased cross section for the major axis and the minor axis is shown in Fig. 9. Four numbers of salient points are shown in Fig. 9a, b. Point A represents the axial strength without any eccentric moment, whereas the flexural strength of the section is shown by point B. Point C is representing the load at the plastic neutral axis and point D is showing the maximum flexural strength capacity when the composite column was loaded by the axial load. From both figures, one can notice that both points C and B are in the same line. That means the maximum flexural strength can be achieved at the neutral axis level. The stress diagram for corresponding salient points A, B, C, and D is shown in Fig. 9c. The notations f_{yc} and f_{yd} are the stresses of the reinforcing bar and rolled steel section respectively. Point A of the interaction diagram is defined as a resistance force against the axial compressive load without any bending moment. The axial load and moment at A can be defined as

$$P_A = f_c bh + f_{ys} A_s + f_{yr} A_{sr} \tag{2}$$

And

$$M_A = 0 \tag{3}$$

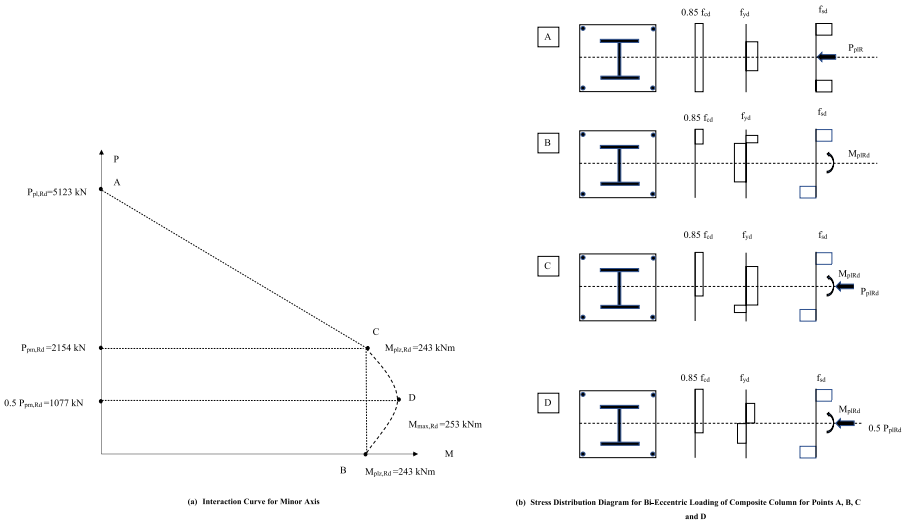

Fig. 9 Load moment interaction curve for major and minor axis

Where, b and h be the width and height of the composite section respectively, A_s is the area of rolled steel section and A_{sr} is the area of the reinforcement bar. Similarly, point D of the interaction diagram is defined as the resistance moment against the eccentricity with the presence of axial compressive force P_D. The axial load and moment at D can be defined as

$$P_D = f_c b \frac{h}{2} \tag{4}$$

$$M_D = f_c \left(\frac{bh^2}{8} \right) + Z_s f_{ys} + f_{yr} A_{sr} \left(d - \frac{h}{2} \right) \tag{5}$$

Where d is the effective depth of composite column and Z_s is the plastic section modulus @ X-axis for rolled steel section. It can be defined as follows:

$$Z_s = \frac{b_f h^2}{4} - \frac{(b_f - t_w) h_w^2}{4} \tag{6}$$

Point B can be defined as the resistance bending moment of the composite section with zero magnitude of axial load, i.e., eccentricity is ∞. If X_u is the depth of neutral axis, the value of X_u can be found out by taking three cases as follows:

Let, b_f = width of flange
t_f = thickness of flange
X_u = depth of neutral axis
b = side of column
d' = effective cover of reinforcement
A_s = area of steel H-section
A_{sr} = area of reinforcement
Φ = diameter of longitudinal reinforcement
Z_s = plastic section modulus of steel H-section
f_c = stress of block concrete
f_{ys} = stress of steel H-section
f_{yr} = stress of longitudinal reinforcement bar

The position of neutral axis for individual case is shown in Fig. 10.

$$Case\ 1 : b_f - t_f \le X_u \le \frac{b}{2}$$

Now,

$$\sum F_B = 0$$

$$f_c b \alpha X_u + \frac{A_s}{2} f_{ys} + \frac{A_{sr}}{2} f_{yr} - \frac{A_s}{2} f_{ys} - \frac{A_{sr}}{2} f_{yr} = 0 \tag{7}$$

$$f_c b \alpha X_u = 0 \tag{8}$$

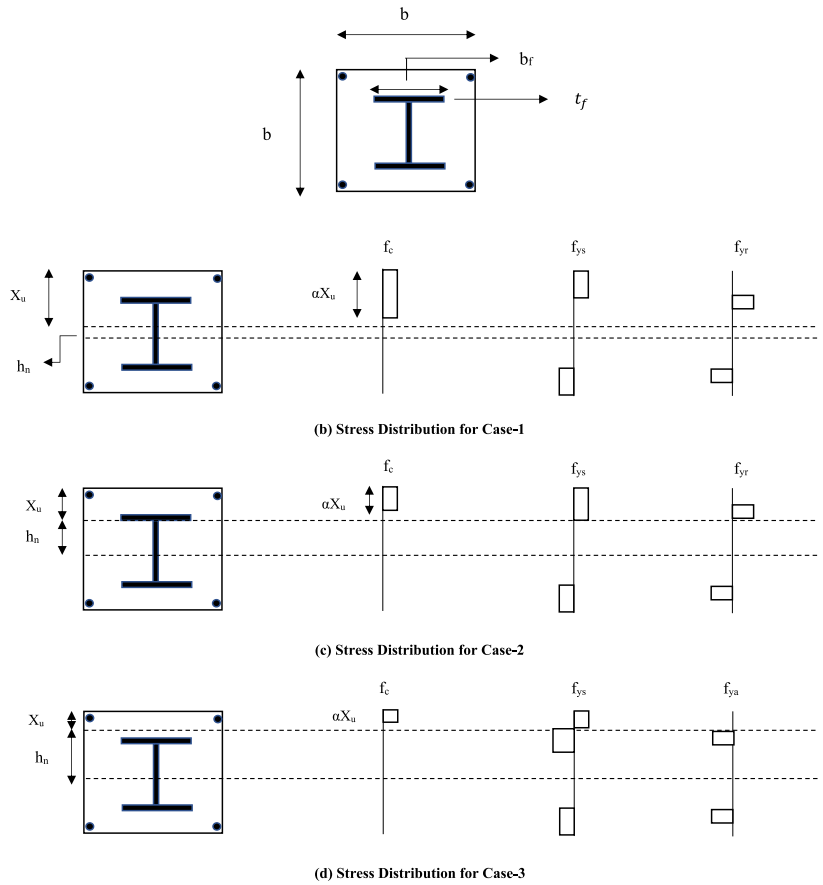

Fig. 10 Stress distribution diagram at point B for different cases

$$X_u = 0 \tag{9}$$

Which is not possible. It indicates that the Case-1 will not be exist practically.

$$\text{Case 2}: \ 0 < X_u < \left(b_f - t_f\right) \text{ and } X_u \geq \left(d' \frac{\varnothing}{2}\right)$$

Again,

$$\sum F_B = 0$$

$$f_c b \alpha X_u + \frac{A_s}{2} f_{ya} + \frac{A_s}{2} f_{yr} - \frac{A_s}{2} f_{ya} - \frac{A_s}{2} f_{yr} - 2\left[t_f f_{ya}\left(b_f - t_f - X_u\right)\right] = 0 \tag{10}$$

$$X_u = \frac{2 t_f f_{ya}\left(b_f - t_w\right)}{f_c b \alpha + 2 t_f f_{ya}} \tag{11}$$

$$h_n = \frac{b}{2} - X_u \tag{12}$$

$$M_B = f_c b\alpha X_u\left(\frac{b}{2} - \frac{\alpha X_u}{2}\right) + Z_s f_{ya} + A_{sr} f_{yr}\left(\frac{b}{2} - d'\right) - \left[2t_f\left(b_f - t_f - X_u\right)f_{ya}\left(\frac{b}{2} - X_u - \left(\frac{b_f - t_f - X_u}{2}\right)\right)\right] \tag{13}$$

Case 3 : $0 < X_u < (b_f - t_f)$ and $X_u \leq \left(d' - \frac{\phi}{2}\right)$

Again,

$$\sum F_B = 0$$

$$f_c b\alpha X_u + \frac{A_s}{2} f_{ya} - A_{sr} f_{yr} - \frac{A_s}{2} f_{ya} - 2\left[t_f\left(b_f - t_f - X_u\right)f_{ya}\right] = 0 \tag{14}$$

$$X_u = \frac{2t_w\left(b_f - t_f\right)f_{ya} + A_{sr} f_{yr}}{f_c b\alpha + 2t_f f_{ya}} \tag{15}$$

Now,

$$h_n = \frac{b}{2} - X_u$$

$$M_B = f_c b\alpha X_u\left(\frac{h}{2} - \frac{\alpha X_u}{2}\right) + Z_a f_{ys} - \left[2t_w\left(b_f - t_f - X_u\right)f_{ya}\left(\frac{b}{2} - X_u - \left(\frac{b_f - t_f - X_u}{2}\right)\right)\right] \tag{16}$$

In Fig. 9a, b, point C refers to the location of neutral axis which shows the same flexural capacity of point B and double of axial load of point D.

For the composite column specimens, the prediction of flexural strength from the plastic stress distribution method defined in EBCS EN 1994-1-1:2014 were found as 6 to 17% greater than from the strain compatibility method described in Eurocode 4. The reason behind this is that the gross section of center-located steel did not yield a large deformation.

Conclusions

The present research was aiming to explore the strength and behavior of fully encased composite columns under bi-axial loading. A total of 36 columns were numerically analyzed to assess the influence of various key parameters such as L/D ratio, e/D ratio, and structural steel contribution ratio; related to the geometry of H-shaped steel column encased by concrete. The following conclusions were drawn from the present research.

(i) The axial load carrying capacity of the composite column was reduced with the increment of the L/D ratio beyond 15.

(ii) Failure occurs by crushing concrete on the compression side and tensile damage of concrete on the tension side, then yielding structural steel and longitudinal rein-

forcement for columns with a lower L/D ratio. For columns with a larger slenderness ratio, the failure mode is only due to tensile damage of concrete and a flexural buckling of the column.

(iii) The ultimate load-carrying capacity and ductility of the fully encased composite columns were enhanced when the structural steel contribution ratio was increased.

(iv) The ultimate load-carrying capacity of fully encased composite columns was gradually reduced due to the increment of the e/D ratio.

(v) EBCS EN1994-1-1:2014 predicted the strength of fully encased composite columns made with normal strength materials regarding a simplified design method by calculating the P-M interaction curve and second-order effects.

Recommendations and future studies

(i) The current study is limited to the bi-axial loading conditions only. An investigation should be done on the behavior and strength of fully encased columns made with normal strength materials under tri-axial and cyclic loading.

(ii) The numerical model may be extended to incorporate the effects of geometric imperfections and residual stresses on the behavior of fully encased composite columns under various loading conditions.

(iii) The present research is limited to H-section steel profile and square shape cross section column. Further investigation is needed with other types of steel profiles and different cross sections.

(iv) Further study is needed to extend the effects of the dynamic loading on the behavior of composite columns with high-strength materials may be investigated.

Abbreviations

L/D	Length to depth ratio
e/D	Eccentricity to depth ratio
δ	Structural steel contribution ratio
FEC	Fully encased composite column
PEC	Partially encased composite column
CFT	Concrete filled tube
CDP	Concrete damage plasticity
FEM	Finite element method
b_f	Width of flange
t_f	Thickness of flange
X_u	Depth of neutral axis
b	Side of column
d'	Effective cover of reinforcement
A_s	Area of steel H-section
A_{sr}	Area of reinforcement
Φ	Diameter of longitudinal reinforcement
Z_s	Plastic section modulus of steel H-section
f_c	Stress of block concrete
f_{ys}	Stress of steel H-section
f_{yr}	Stress of longitudinal reinforcement bar

Acknowledgements

Our grateful acknowledgment goes to Wollega University for its extensive support.

Authors' contributions

BR analyzed results and prepared manuscript. FK assembled the composite column specimen by ABAQUS. BD had written the literature review. SG had written the literature review. KK had edited the manuscript and checked the

grammatical mistakes. EM contributed the conclusions and recommendations chapter. All authors have read and approved the manuscript.

Funding
No funding was received for present research.

Availability of data and materials
Some or all data, models, or code that support the findings of this study are available from the corresponding author upon reasonable request.

Declarations

Competing interests
The authors declare that they have no competing interests.

Received: 11 October 2022 Accepted: 13 December 2022
Published online: 28 December 2022

References

1. Mirza SA, Skrabek BW (1991) Reliability of short composite beam-column strength interaction. J Struct Eng. 117(8):2320–2339. https://doi.org/10.1061/(ASCE)0733-9445(1991)117:8(2320)
2. Wu B, Jian S-M, Zhao X-Y (2019) Structural behavior of steel-concrete partially encased composite columns containing demolished concrete lumps under axial compression. Eng Struct. 197:109383. https://doi.org/10.1016/j.engstruct.2019.109383
3. Lu Y, Li N, Li S, Liang H (2015) Behavior of steel fiber reinforced concrete-filled steel tube columns under axial compression. Constr Build Mater. 95:74–85. https://doi.org/10.1016/j.conbuildmat.2015.07.114
4. Tokgoz S, Dundar C, Tanrikulu AK (2012) Experimental behaviour of steel fiber high strength reinforced concrete and composite columns. J Constr Steel Res 74:98–107. https://doi.org/10.1016/j.jcsr.2012.02.017
5. Shanmugam NE, Lakshmi B (2001) State of the art report on steel–concrete composite columns. J Constr Steel Res 57(10):1041–1080. https://doi.org/10.1016/S0143-974X(01)00021-9
6. Ellobody E, Young B, Lam D (2011) Eccentrically loaded concrete encased steel composite columns. Thin-Walled Struct. 49(1):53–65. https://doi.org/10.1016/j.tws.2010.08.006
7. Chen C-C, Lin N-J (2006) Analytical model for predicting axial capacity and behavior of concrete encased steel composite stub columns. J Constr Steel Res 62(5):424–433. https://doi.org/10.1016/j.jcsr.2005.04.021
8. En CEN (1994) 1-1, Eurocode 4: Design of composite steel and concrete structures, Part 1-1 Gen. rules rules Build
9. C. B. S. Committee (2016) National Standard of the People's Republic of China: Code for Design of Composite Structures (JGJ 138-2016). China Archit. Build. Press, Beijing
10. Rath B, Agon EC, Dereje B, Garoma S, Debela A, Kebede K, Yadeta R (2023) Modification of load carrying capacity model for composite column. J Build Pathol Rehabil. 8(1):1–18. https://doi.org/10.1007/s41024-022-00256-0
11. Nasery MM, Hüsem M, Okur FY, Altunişik AC (2020) Numerical and experimental investigation on dynamic characteristic changes of encased steel profile before and after cyclic loading tests. Int J Civ Eng. 18(12):1411–1431. https://doi.org/10.1007/s40999-020-00545-0
12. Nasery MM, Ağcakoca E, Yaman Z (2020) Experimental and numerical analysis of impactor geometric shape effects on steel beams under impact loading. Structures 27:1118–1138. https://doi.org/10.1016/j.istruc.2020.07.012
13. An Y-F, Han L-H, Roeder C (2015) Performance of concrete-encased CFST box stub columns under axial compression. Structures 3:211–226. https://doi.org/10.1016/j.istruc.2015.05.001
14. Wang H, Li J, Song Y (2019) Numerical study and design recommendations of eccentrically loaded partially encased composite columns. Int J Steel Struct 19(3):991–1009. https://doi.org/10.1007/s13296-018-0179-7
15. Rath B, Garoma S, Kudama R, Agon EC, Tadese T, Gutema EM (2022) Effect of different width ratio and transversal link pattern on the load carrying capacity of partially encased composite column. Asian J Civ Eng:1–14. https://doi.org/10.1007/s42107-022-00498-w
16. Zhou X, Yan B, Liu J (2015) Behavior of square tubed steel reinforced-concrete (SRC) columns under eccentric compression. Thin-Walled Struct. 91:129–138. https://doi.org/10.1016/j.tws.2015.01.022
17. Rodrigues JPC, Correia AJM, Pires TAC (2015) Behaviour of composite columns made of totally encased steel sections in fire. J Constr Steel Res 105:97–106. https://doi.org/10.1016/j.jcsr.2014.10.030
18. Campian C, Nagy Z, Pop M (2015) Behavior of fully encased steel-concrete composite columns subjected to monotonic and cyclic loading. Procedia Eng. 117:439–451. https://doi.org/10.1016/j.proeng.2015.08.193
19. Abdulla NA (2020) Mechanical behavior of slender composite columns under axial compression load. KSCE J Civ Eng 24(1):208–218. https://doi.org/10.1007/s12205-020-0669-y
20. Ekmekyapar T, Al-Eliwi BJM (2016) Experimental behaviour of circular concrete filled steel tube columns and design specifications. Thin-Walled Struct. 105:220–230. https://doi.org/10.1016/j.tws.2016.04.004
21. Gunawardena Y, Aslani F (2021) Finite element modelling of concrete-filled spiral-welded mild-steel tube short and long columns. Structures 30:1020–1041. https://doi.org/10.1016/j.istruc.2021.01.074
22. Gourley BC, Tort C, Hajjar JF, Schiller PH (2001) A synopsis of studies of the monotonic and cyclic behaviour of concrete-filled steel tube beam-columns. University of Minnesota, Minneapolis
23. Minh H-L, Khatir S, Wahab MA, Cuong-Le T (2021) A concrete damage plasticity model for predicting the effects of compressive high-strength concrete under static and dynamic loads. J Build Eng. 44:103239. https://doi.org/10.1016/j.jobe.2021.103239

24. EBCS- 4 Part 1-1 SE (2014), Design of composite steel and concrete structures Part 1-1 : General rules and rules for buildings.
25. Dundar C, Tokgoz S, Tanrikulu AK, Baran T (2008) Behaviour of reinforced and concrete-encased composite columns subjected to biaxial bending and axial load. Build Environ. 43(6):1109–1120. https://doi.org/10.1016/j.buildenv.2007.02.010

Publisher's Note